Chemical Engineering Journal 341 (2018) 126–136

Contents lists available at ScienceDirect

Chemical Engineering Journal

journal homepage: www.elsevier.com/locate/cej

Insights into atrazine degradation by persulfate activation using composite of nanoscale zero-valent iron and graphene: Performances and mechanisms

Shaohua Wu[a,1], Huijun He[a,1], Xiang Li[a,1], Chunping Yang[a,b,*], Guangming Zeng[a], Bin Wu[a], Shanying He[b], Li Lu[b,*]

[a] College of Environmental Science and Engineering, Hunan University and Key Laboratory of Environmental Biology and Pollution Control (Hunan University), Ministry of Education, Changsha, Hunan 410082, China
[b] Zhejiang Provincial Key Laboratory of Waste Treatment and Recycling, College of Environmental Science and Engineering, Zhejiang Gongshang University, Hangzhou, Zhejiang 310018, China

HIGHLIGHTS

- Atrazine was efficiently degraded by nZVI/GR-PS system.
- The effects of various operational parameters on atrazine degradation were evaluated.
- Both sulfate radical and hydroxyl one were produced on the surface of nZVI/GR, while sulfate radical was predominant.
- The degradation performance in actual water was studied.
- Mechanisms and pathways for atrazine degradation were examined and proposed.

ARTICLE INFO

Keywords:
Zero-valent iron
Graphene
Herbicide
Atrazine
Radical
Advanced oxidation process

ABSTRACT

Atrazine, a herbicide used widely, could not be effectively removed from waters by chemical or biological processes. In this work, the performances and mechanisms for atrazine degradation were examined by persulfate (PS) activation with nanoscale zero-valent iron (nZVI) and graphene (GR) composites at various conditions including dosages of nZVI/GR and PS, pH value, temperature and natural organic matters (NOM). Results showed that mass ratio of 5:1 for nZVI to GR exhibited the highest efficiency for catalytic degradation of atrazine when 92.1% of atrazine was removed within 21 min. The degradation efficiencies of atrazine increased when PS concentration increased from 0.2 to 1.0 mM, and were favored in acidic pH and high temperature, while was not affected by NOM with a concentration less than 4 mg/L. Electron spin resonance and radical quenching studies showed that both $\cdot OH$ and $SO_4^{\cdot -}$ were mainly produced on the surface of nZVI/GR, while $SO_4^{\cdot -}$ was the predominant radicals responsible for the degradation of atrazine. Mechanisms for atrazine degradation were also proposed on the basis of XRD and XPS analysis. And its degradation pathways involved in dealkylation, alkylic hydroxylation, dechlorination-hydroxylation, and alkylic oxidation using LC/MS/MS techniques. These results could provide a better understanding of the application of nZVI/GR-PS system for atrazine removal from waters.

1. Introduction

Atrazine (2-chloro-4-ethylamino-6-isopropylamino-s-triazine) was a widely used herbicide for the control of broad leaf and grassy weeds. It could cause carcinogenic and endocrine-disrupting effects even at relatively low concentrations [1,2]. Atrazine and its metabolites have been frequently detected in surface and ground waters due to its high mobility and moderate aqueous solubility [3–6]. Consequently, atrazine pollution and its control have been paid close attention [7,8]. Unfortunately, various treatment methods including adsorption,

---

Abbreviations: $SO_4^{\cdot -}$, sulfate radical; $\cdot OH$, hydroxyl radical; nZVI, nanoscale zero-valent iron; PS, persulfate; GR, graphene; rGO, reduced graphene oxide; NOM, natural organic matters; DMPO, 5, 5-Dimethyl-1-pyrroline N-oxide; L, lepidocrocite; M, magnetite/maghemite; ESR, electron spin resonance; TBA, *Tert*-butanol; MeOH, methanol; TOC, Total organic carbon; LC-MS-MS, liquid chromatography-mass spectrometry-mass spectrometry; HPLC, high performance liquid chromatography; FTIR, Fourier transform infrared spectroscopy; EDS, energy-dispersive X-ray spectroscopy; SEM, scanning electron microscopy; TEM, transmission electron microscopy; XRD, X-ray powder diffraction; XPS, X-ray photoelectron spectroscopy

[*] Corresponding authors at: College of Environmental Science and Engineering, Hunan University, Changsha, Hunan 410082, China.
E-mail addresses: yangc@hnu.edu.cn (C. Yang), LL0106@zjgsu.edu.cn (L. Lu).

[1] These authors contribute equally to this article.

https://doi.org/10.1016/j.cej.2018.01.136
Received 5 October 2017; Received in revised form 24 January 2018; Accepted 25 January 2018

biodegradation, and chemical oxidation could not effectively remove atrazine from water [9–12]. For example, *Pseudomonas* sp. Strain ADP was difficult to survive in atrazine alone, because it was just capable of using atrazine as a nitrogen source, rather than as the energy source [9]. Therefore, it is urgently required to develop an effective method to remove atrazine from water.

In recent years, many reports on sulfate radicals ($SO_4^{\cdot -}$)-based advanced oxidation processes are available for the degradation of organic contaminants [13–16]. Compared with hydroxyl radicals ($\cdot OH$), $SO_4^{\cdot -}$ was more effective to oxidize organic pollutants due to its high redox potential (2.5–3.1 V) and selectivity [17–19]. Usually, $SO_4^{\cdot -}$ could be generated from the activation of persulfate (PS) by heat [13], ultrasound [20], UV light [21,22], bases [23], transition metals [24–26], or metal-free carboncatalysts [27,28]. Nonetheless, these methods have their own limitations. Some of them either need to be further improved to increase removal efficiency, or may cause serious secondary pollution to the environment.

Recently, nanoscale zero-valent iron (nZVI) has been employed to activate PS for the degradation of contaminants such as DDTs, bisphenol A and trichloroethene, because it is high efficient, cost-effective, and environmentally friendly material [29–32]. For example, 97% of trichloroethene was removed at nZVI/PS molar ratio of 1:2 within 360 min [29]. However, nZVI was easily oxidized and thus generated a large amount of Fe^{2+} in a short time. Subsequently, the rapid consumption of $SO_4^{\cdot -}$ by excess Fe^{2+} and a rapid conversion of Fe^{2+} to Fe^{3+} in the nZVI/PS system decreased the removal efficiency of contaminants [29,32]. nZVI was also prone to aggregation, reducing its catalytic activity. To address this problem, graphene (GR), as a two-dimensional monolayer of sp^2-bonded carbon atoms, was used for the immobilization of nZVI due to its large specific surface area, charge transportation and mechanical strength [33,34]. The presence of reduced graphene oxide (rGO) retarded the corrosion of nZVI and benefited the electron transfer between nZVI and contaminants [35,36]. Furthermore, ZVI/GR composites were prepared and showed excellent ability to activate PS for the degradation of trichloroethylene [37]. Although they investigated the effects of various parameters on nZVI/rGO-PS system, its activation mechanisms still remained unknown, especially the role of rGO in the formation of free radicals. As reported by Duan et al. [27], rGO was demonstrated to effectively activate PS for the catalytic oxidation of phenol, and was even comparable to the most efficient electron donor of nZVI. In addition, limited information on the removal of atrazine by nZVI/GR-PS system is available, and degradation mechanism has not been elucidated.

In this work, nZVI/GR composites were synthesized and applied in the activation of PS for atrazine degradation. The objectives of this work were: 1) to prepare and characterize nZVI/GR composites; 2) to evaluate the performances of the composites for atrazine degradation at various conditions including PS and nZVI/GR doses, pH value, natural organic matters (NOM), and temperature; 3) to identify the dominant reactive species by the quenching tests and electron spin resonance (ESR); and 4) to propose the activation mechanisms and degradation pathways for atrazine oxidation.

2. Materials and methods

2.1. Chemical reagents

Graphite powder, sodium persulfate ($Na_2S_2O_8$), sodium borohydride ($NaBH_4$, > 98%), ferrous sulfate ($FeSO_4{\cdot}7H_2O$, 99.7%), sodium thiosulfate ($Na_2S_2O_3{\cdot}5H_2O$, > 99.0%), humic acid (used as NOM), methanol (MeOH), and *Tert*-butanol (TBA, ≥99.8%) were purchased from Sinopharm Chemical Reagent Co., Ltd. Atrazine ($C_8H_{14}N_5Cl$, 99.0%) and 5, 5-Dimethyl-1-pyrroline N-oxide (DMPO, > 97.0%) was obtained from Aladdin Chemistry Co., Ltd. All other reagents were of analytical grade and prepared in Milli-Q water (18.2 MΩ·cm). Real water samples were collected from Xiangjiang River and Taozi Lake (Changsha, China) and stored at 4 °C. Atrazine solutions (20 mg/L) were prepared by magnetically stirring 48 h in Milli-Q water prior to the experiment.

2.2. Preparation and characterization of nZVI/GR

GO was synthesized by oxidizing graphite powder according to the Hummers method [38]. The nZVI/GR composites were prepared as follows: a certain amount of GO and 200 mL methanol/water (3/7, v/v) were added to 500 mL three-necked flask and ultrasonically stirred for 20 min. Then, 2.0 g $FeSO_4{\cdot}7H_2O$ was added into the above solution for another 40 min. Subsequently, 100 mL of $NaBH_4$ solution (1.2 g) was dropwise added with vigorous stirring under nitrogen atmosphere. After the $NaBH_4$ solution was drained, the mixture was stirred continuously for 30 min. Finally, the prepared composites were collected by vacuum filtration and rinsed with Milli-Q water for several times. The obtained products were vacuum-dried at 50 °C overnight. The nZVI/GR composites with different mass ratios of GO to nZVI (1:40, 1:20, 1:10, 1:5) were obtained by changing the amount of GO.

The crystallinity of the samples was characterized by X-ray powder diffraction (XRD, Rigaku) with Cu Kα radiation. The morphologies were observed by scanning electron microscopy with energy-dispersive X-ray spectroscopy (SEM-EDS, Quanta-200, FEI) and transmission electron microscopy (TEM, TecnaiG2 F20, FEI). Fourier transform infrared spectroscopy (FTIR) was recorded on a Nicolet 6700 spectrometer. The surface elemental compositions were analyzed by X-ray photoelectron spectroscopy (XPS, Thermo Fisher-VG Scientific) with Al Kα X-ray source.

2.3. Experimental procedures

All experiments were conducted in 250 mL sealed conical flask with a rotary shaker (150 rpm, 25 °C). The reactions were initiated by adding specified amount of nZVI or nZVI/GR to 100 mL of mixture solutions containing atrazine (10 mg/L) and PS (0.5 mM). 1 mL samples were collected at predefined time intervals and filtered through 0.45 μm membrane filters. Then, 10 μL of 1 M $Na_2S_2O_3$ was added to quench the reaction. The filtered solution was analyzed for atrazine concentration.

Several sets of the experiments were conducted to determine the effects of various parameters (PS and nZVI/GR doses, pH, NOM, temperature) on atrazine degradation. The solution pH was adjusted to 6.0 ± 0.1 using 0.1 M NaOH or HCl unless specially mentioned. To identify the contribution of the reactive species in nZVI/GR-PS system, MeOH, TBA, and phenol were used as radical scavengers. To test the reusability of nZVI/GR, it was collected by centrifugation and washed with Milli-Q water after each cycle, and then reused by adding fresh PS and atrazine. All experiments were run in triplicate, and the standard deviations were shown.

2.4. Analytical methods

Atrazine concentrations were determined by high performance liquid chromatography (HPLC, Agilent) equipped with UV detector at the wavelength of 230 nm and SB-C18 reverse phase column (4.6 × 250 mm, 5 μm). The mobile phase consisted of methanol, water and acetonitrile (60/30/10, v/v/v) at a flow rate of 1 mL/min. Column temperature was set at 40 °C. Total organic carbon (TOC) was determined by TOC-5050A analyzer (Shimadzu, Japan). The concentrations of Fe(II) and Fe(III) were detected at 510 nm by a 1,10-phenanthroline method with Hach DR 2800 portable spectrophotometer. The degradation products were identified by liquid chromatography-mass spectrometry- mass spectrometry (LC-MS-MS, Agilent 1290 series LC, 6460 Triple Quad LC/MS) according to the method [39] with some modification. Detailed methods were described in the Supplementary Information (Text S1). The free radicals in the nZVI/GR-PS system were detected by electron spin resonance (ESR, JES FA200, JEOL), and its setting was shown in Text S2.

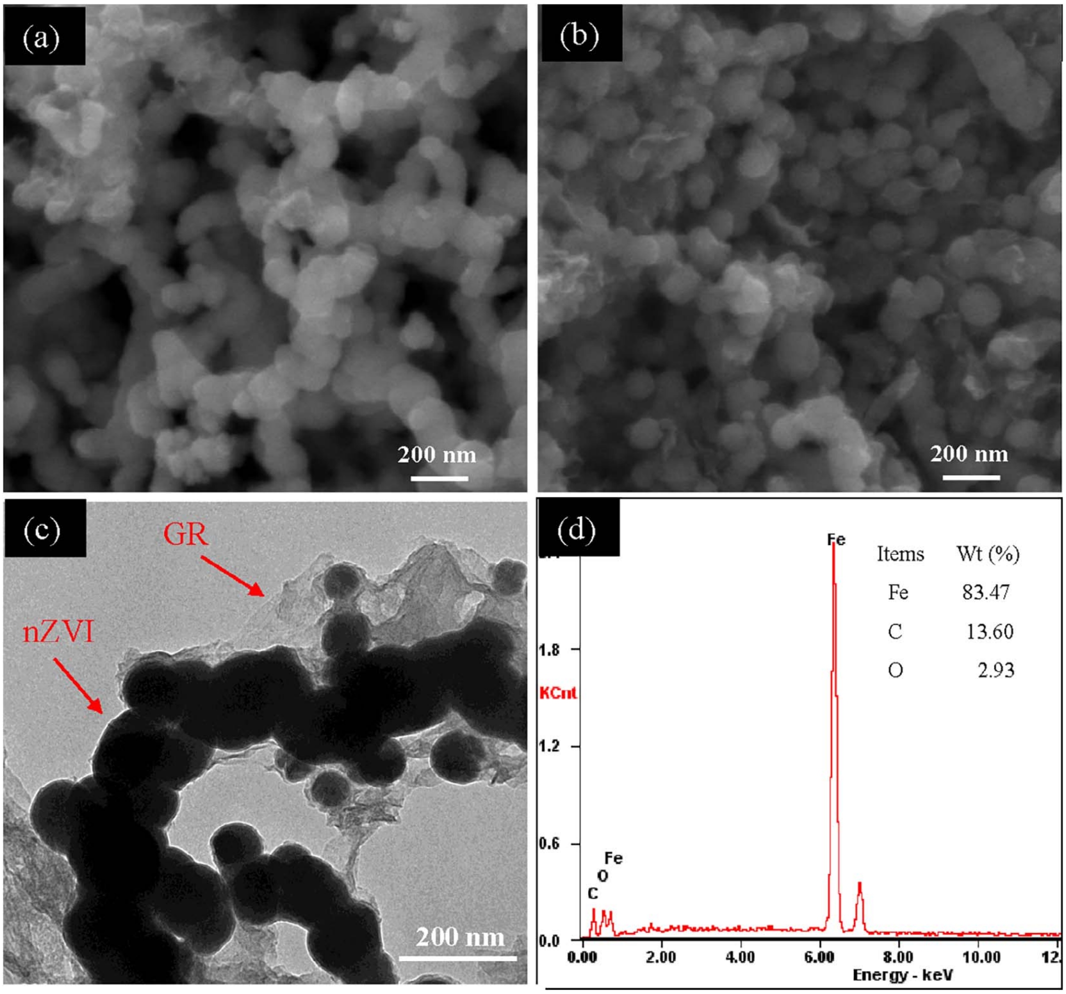

Fig. 1. SEM spectra of nZVI (a), SEM spectra of nZVI/GR(5:1), TEM spectra of nZVI/GR(5:1) (c), EDS spectra of (5:1) (d).

3. Results and discussion

3.1. Characterization of nZVI/GR

SEM images showed that nZVI alone was spherical and formed a chain-like structure (Fig. 1a). As for nZVI/GR (5:1), nZVI was dispersed on the surface of GR with a relatively uniform distribution (Fig. 1b), which could be further confirmed by TEM. It could be also seen that the size of nZVI on nZVI/GR (5:1) was about 120 nm (Fig. 1c). In addition, the element compositions of nZVI/GR (5:1) by EDS analysis were Fe, C, and O, and their contents were respectively 83.47%, 13.60%, and 2.93%, which was well consistent with the theoretical mass ratio of 5:1 (Fig. 1d).

The XRD patterns of the samples were shown in Fig. 2a. For nZVI and nZVI/GR, the only peak at 44.5° should be assigned to nZVI (JCPDS 06-0696). This could be further verified by XPS (Fig. 2b). XPS spectra illustrated that shoulder peak at 707.1 eV was corresponded to nZVI ($2p_{3/2}$), and its signal was relatively weak due to the high surface sensitivity of XPS (less than 10 nm in depth). The FTIR spectra of GO and nZVI/GR (5:1) were shown in Fig. 2d. For GO, the peaks observed at 1720 cm^{-1}, 1624 cm^{-1} and 1400 cm^{-1} were corresponded to the stretching vibration of C=O, C=C and C=O–O, respectively. The characteristic peaks around 1225 cm^{-1} and 1044 cm^{-1} were related to the stretching vibration of epoxy (C–O–O and C–O) and alkoxy groups (C–O), respectively. However, the above peaks were not observed in the nZVI/GR. Moreover, the typical characteristic peak of GO reported by Li et al. [40] at 10.9° was also not detected in the nZVI/GR (Fig. 2a). These results showed that GO was reduced to GR and nZVI/GR composites were successfully prepared.

3.2. Atrazine removal

The removal of atrazine by nZVI, GR, and nZVI/GR with different mass ratios in the absence and presence of PS was shown in Fig. 3. PS alone could hardly remove atrazine. nZVI and nZVI/GR particles exerted little influence on atrazine removal, suggesting that the adsorption was negligible. Degradation efficiency of 66.1% was observed in nZVI/PS system, while 49.7% was obtained in Fe^{2+}/PS system, indicating that nZVI was more effective in activating PS than Fe^{2+} ion. Similar result was found for the degradation of DDTs using nZVI/PS system [30]. Degradation efficiency of 36.7% was obtained in the GR-PS system, which was higher than the sum of GR and PS alone (23.8%). Furthermore, the degradation of atrazine was significantly increased in the nZVI/GR-PS system compared to nZVI/PS system. These results indicated that GR might stimulate PS decomposition. In the presence of PS, the degradation of atrazine was enhanced as the increase of mass ratio of nZVI/GR, especially degradation efficiency of 92.1% occurred within 21 min at nZVI/GR with mass ratio of 5:1, which was similar to that reported by Yan et al. [41]. This might be due to the greater specific surface area and the more active sites by the oxygen-containing functional groups of GR, which facilitated the generation of $SO_4^{\cdot-}$. Bekris et al. [42] reported that GR could be effectively used as an activator of PS for the effective oxidation of micro-pollutants. In addition, rGO was demonstrated superior efficiency toward PS activation for

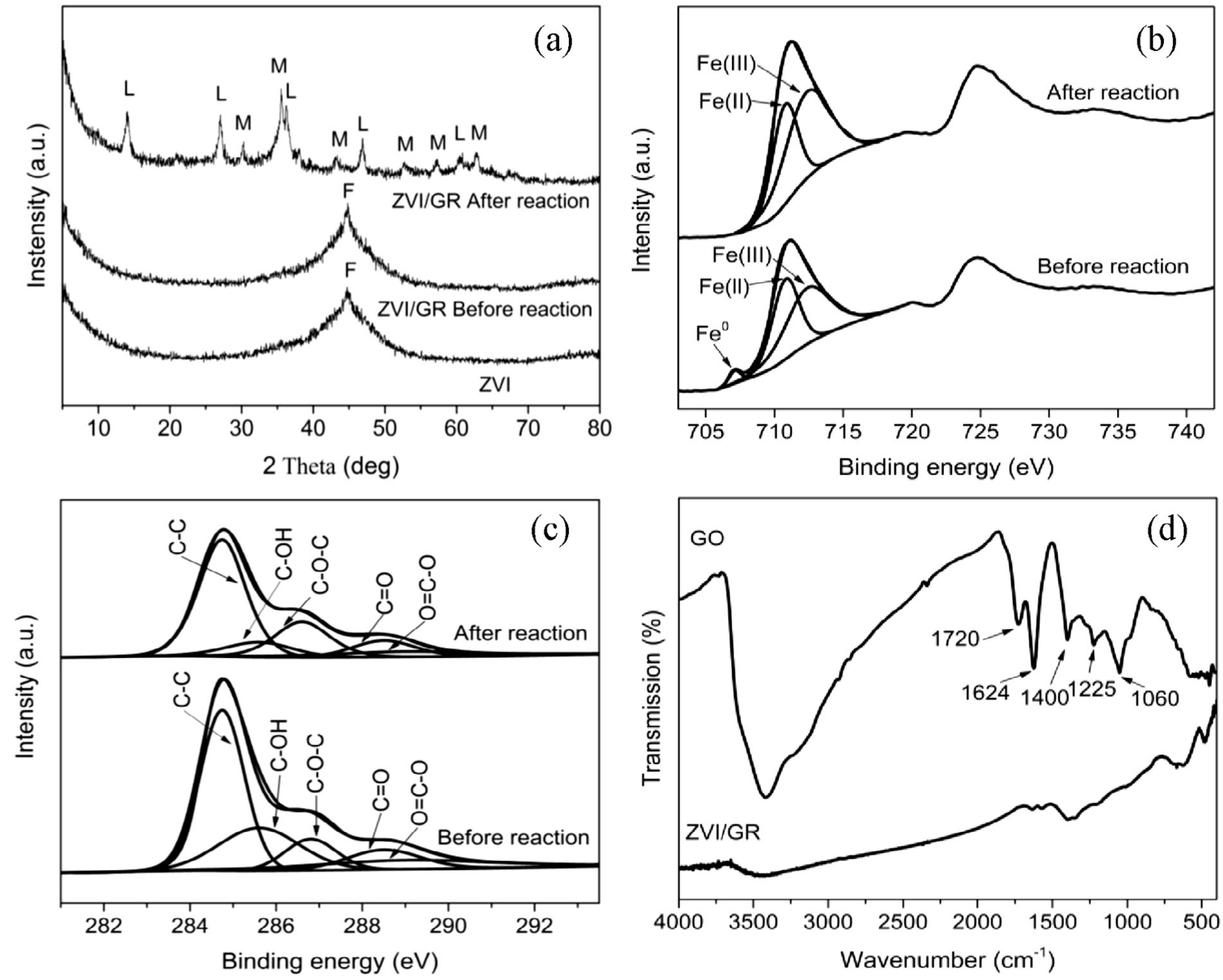

Fig. 2. XRD patterns of nZVI and nZVI/GR (a), XPS spectra of nZVI/GR before and after reaction: Fe 2p spectra (b), C 1 s spectra (c), FTIR spectra of GO and nZVI/GR (d).

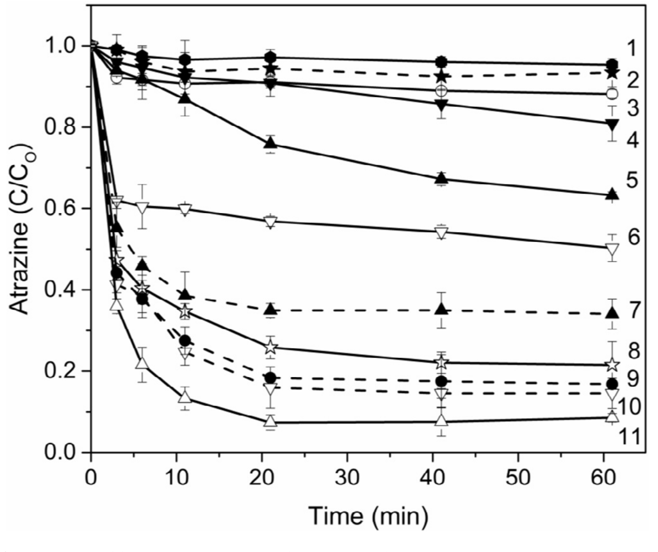

Fig. 3. Removal kinetic of atrazine in the systems of (1) PS, (2) nZVI, (3) nZVI/GR (5:1), (4) GR, (5) GR-PS, (6) Fe^{2+}-PS, (7) nZVI-PS, (8) nZVI/GR(40:1)-PS, (9) nZVI/GR(20:1)-PS, (10) nZVI/GR(10:1)-PS, and (11) nZVI/GR(5:1)-PS. Conditions: [PS] = 0.50 mM, [catalysts] = 0.10 g/L, [atrazine] = 10 mg/L, T = 25 °C, pH = 6.0.

phenol oxidation, and was even comparable to the most efficient electron donor of nZVI [27]. They further proposed that rGO served as an excellent electron bridge to facilitate the fast electron-transfer processes. Yan et al. [41] also showed that both the redox effect coupled in Fe_3O_4 and the electron transfer by oxygen-containing functional groups on rGO surface enhanced the generation of $SO_4^{\cdot -}$. These results clearly showed that nZVI/GR was better than nZVI as an efficient PS activator for atrazine degradation.

3.3. Influences of several parameters on atrazine degradation

3.3.1. Effects of PS and nZVI/GR doses

To comprehensively evaluate the degradation performance of nZVI/GR, the effects of PS concentration, nZVI/GR dosage, pH value, NOM and temperature were investigated. The degradation of atrazine was significantly affected by the concentrations of PS (Fig. 4a). As PS concentration increased from 0.2 to 0.4 mM, the degradation efficiency of atrazine was rapidly increased from 34.2% to 79.5%. Although the degradation efficiency of atrazine at 1.0 mM was lower than that at 0.8 mM within 21 min, atrazine was completely degraded at 1.0 mM after 41 min. When PS concentration further increased to 2.5 mM, its degradation efficiency dropped to 86.8% after 61 min, and its degradation change was similar to that at 0.4 mM PS. This was attributed to more $SO_4^{\cdot -}$ produced with the increase of PS concentration (Eq. (1)), but high levels of $SO_4^{\cdot -}$ could be consumed by itself and excess PS (Eqs. (2) and (3)), leading to the decreased degradation.

$$S_2O_8^{2-} + Fe^{2+} \rightarrow SO_4^{2-} + SO_4^{\cdot -} + Fe^{3+} \quad k = 3.0 \times 10^1\ M^{-1}\ s^{-1} \tag{1}$$

$$SO_4^{\cdot -} + SO_4^{\cdot -} \rightarrow S_2O_8^{2-} \quad k = 4.0 \times 10^8\ M^{-1}\ s^{-1} \tag{2}$$

$$S_2O_8^{2-} + SO_4^{\cdot -} \rightarrow S_2O_8^{\cdot -} + SO_4^{2-} \quad k = 6.1 \times 10^5\ M^{-1}\ s^{-1}$$

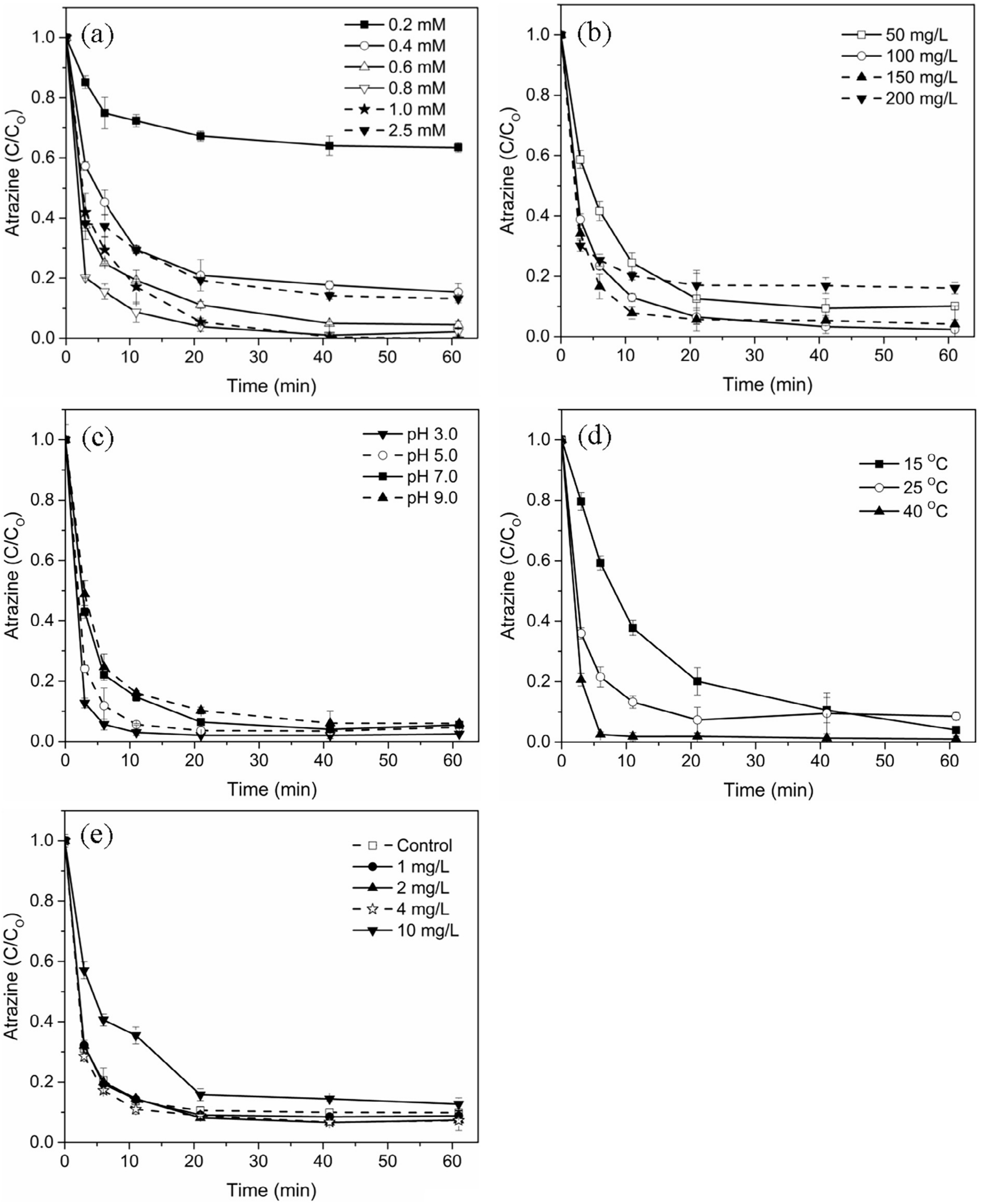

Fig. 4. The influencing factors on the degradation performance of nZVI/GR-PS: (a) PS concentration, (b) nZVI/GR dosage, (c) initial pH, (d) temperature, (e) NOM. Conditions: [PS] = 0.50 mM, [nZVI/GR] = 0.10 g/L, [atrazine] = 10 mg/L, T = 25 °C, pH = 6.0; humic acid was expressed as TOC (mg/L).

(3)

$$Fe^0 + S_2O_8^{2-} \rightarrow Fe^{2+} + 2SO_4^{2-} \quad (4)$$

$$Fe^0 + 2Fe^{3+} \rightarrow 3Fe^{2+} \quad (5)$$

$$Fe^{2+} + SO_4^{\cdot -} \rightarrow Fe^{3+} + SO_4^{2-} \quad k = 4.6 \times 10^9\ M^{-1}\ s^{-1} \quad (6)$$

nZVI/GR dose had a positive effect on the degradation of atrazine before it increased to 150 mg/L (Fig. 4b). The increase of nZVI/GR dose would generate more $SO_4^{\cdot -}$, which enhanced the degradation efficiency of atrazine (Eqs. (1) and (4)). Nevertheless, as its dose further increased to 200 mg/L, the degradation efficiency decreased. Degradation efficiency of 83.0% was obtained within 21 min and then remained unchanged. On one hand, excessive Fe^{2+} released from nZVI/GR at a relatively high dosage would consume large amount of $SO_4^{\cdot -}$ (Eqs. (5) and (6)). In addition, more nZVI/GR doses in solution resulted in an increased aggregation itself, thus reducing the total active sites

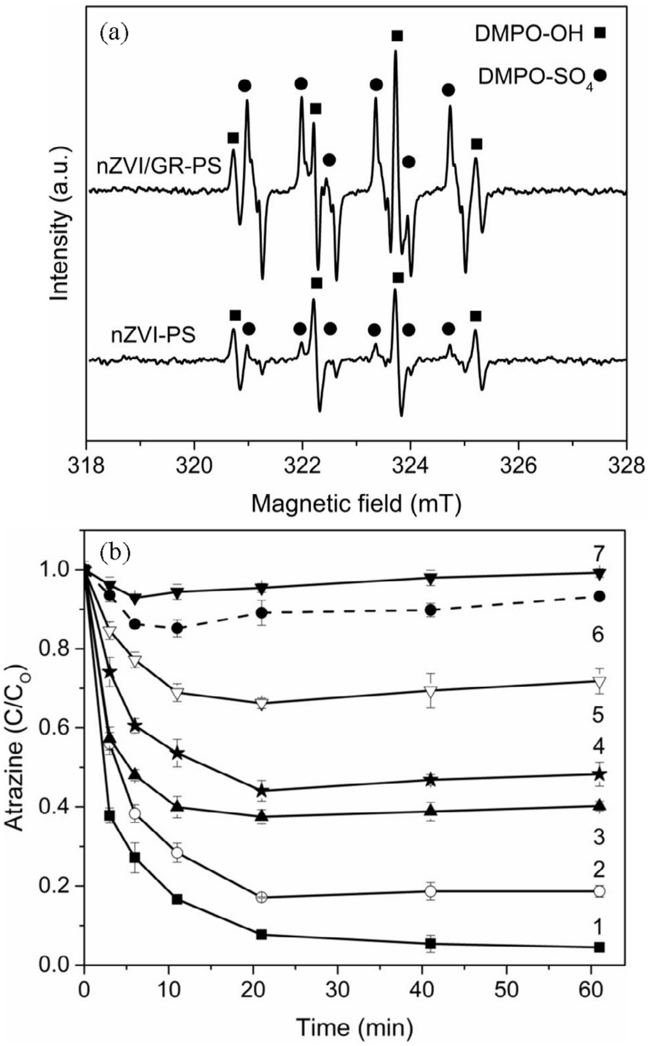

Fig. 5. (a) ESR spectrums of DMPO-SO4 and DMPO-OH in the nZVI-PS or nZVI/GR- PS systems at 5 min; 1 mT = 10 G. (b) Effects of (1) Control, (2) 50 mM TBA, (3) 50 mM MeOH, (4) 500 mM TBA, (5) 500 mM MeOH, (6) 5.0 mM Phenol, and (7) 50 mM Phenol on atrazine degradation. Conditions: [PS] = 0.50 mM, [nZVI/GR] = 0.10 g/L, [atrazine] = 10 mg/L, [DMPO] = 100 mM, T = 25 °C, pH = 6.0.

[43].

3.3.2. Effect of pH

The effect of initial pH on atrazine degradation by ZVI/GR-PS was investigated. As shown in Fig. 4c, acidic pH was favorable for atrazine degradation. Especially, within 3 min, degradation efficiencies of 87.2%, 75.9%, 56.1% and 51.1% were achieved at pH 3, 5, 7, and 9, respectively. Previous work reported that the pKa of atrazine was 1.7 [44,45], thereby the charge of atrazine was negative within the pH range of this study. At acidic condition, more dissolved Fe^{2+} was generated from nZVI/GR, which could promote PS decomposition to generate $SO_4^{\cdot -}$. Conversely, the release of iron ions would slow down and precipitate under neutral and alkaline conditions, which resulted in the formation of iron hydroxides and further hindered the release of Fe^{2+}. Wei et al. [46] concluded two reasons responsible for the low activation efficiency of PS by nZVI at high pH. In addition, $SO_4^{\cdot -}$ would transform into $\cdot OH$ at alkaline condition [23]. Lutze et al. [47] showed that the reaction of atrazine with $SO_4^{\cdot -}$ would be faster than that with $\cdot OH$ ($k_{SO_4^{\cdot -}} = 4.2 \times 10^9\, M^{-1} s^{-1}$, $k_{\cdot OH} = 2.4–3.0 \times 10^9\, M^{-1} s^{-1}$). Thereby, the degradation of atrazine was favored in acidic pH. After 41 min, the degradation efficiency of atrazine were almost the same at different pH values. It might attribute to the decreased pH (pH < 5) (Table S1), which alleviated the inhibiting effect of high pH on $SO_4^{\cdot -}$ generation. The iron leaching also further confirmed the above explanation (Table S1). Even at initial pH 9.0, the iron leaching reached 10.21 mg/L. The decreased pH value as reaction processed was due to the accumulation of H^+, which was explained by Wei et al. [46].

$$Fe^0 + 2H^+ \rightarrow Fe^{2+} + H_2 \quad (7)$$

$$SO_4^{\cdot -} + OH^- \rightarrow SO_4^{2-} + \cdot OH \quad k = 6.5 \times 10^7 M^{-1} s^{-1} \quad (8)$$

3.3.3. Effect of temperature

The effect of temperature on atrazine degradation by nZVI/GR-PS was shown in Fig. 4d. As the temperature rose, the degradation of atrazine was significantly enhanced. Especially, complete degradation of atrazine was obtained at 40 °C within 41 min. Meanwhile, the control experiment using 0.5 mM of PS alone was carried out at same temperatures (Fig. S1). The degradation efficiency of atrazine with PS alone was 2.4%, 8.8% and 11.5% at 15 °C, 25 °C and 40 °C, respectively. The result indicated that heat energy could activate PS to generate $SO_4^{\cdot -}$ (Eq. (9)), which was responsible for the degradation of atrazine. This was consistent with the study reported by Ji et al. [13], who found that 50 μM atrazine could be completely degraded at 60 °C, in the presence of 1 mM PS. Moreover, the degradation efficiency of atrazine by ZVI/GR-PS was much higher than by PS alone at any temperatures. Synergistic activation of PS by heat and nZVI was found to effectively enhance the oxidation of polyvinyl alcohol [32]. Furthermore, high temperature could promote the corrosion of nZVI and thus released more Fe^{2+} into aqueous solution, producing more $SO_4^{\cdot -}$.

$$S_2O_8^{2-} + heat \rightarrow 2\, SO_4^{\cdot -} \quad (9)$$

3.3.4. Effect of NOM

NOM was ubiquitous in waters, which could act as radical scavenger via competing for $\cdot OH$ and $SO_4^{\cdot -}$ [48]. Humic acid, a major constituents of NOM, contained carbonyl, carboxylate, phenol, and hydroxyl groups, which could be adsorbed onto catalyst and blocked reactive sites, thus inhibiting the oxidation process [49]. In this study, humic acid was used to evaluate the effect of NOM on atrazine degradation (Fig. 4e). As shown in Fig. 2e, the presence of NOM was favorable for atrazine degradation at low concentrations (< 4.0 mg/L as TOC). This might be contributed to the oxygen- containing functional groups of humic acid, which would activate PS to generate free radicals. Previous studies reported that semiquinone radicals, formed from phenol or quinones, could efficiently stimulate PS to generate $SO_4^{\cdot -}$ [50]. Moreover, atrazine was degraded more efficiently by $SO_4^{\cdot -}$ than by $\cdot OH$, in the presence of NOM [47]. This has been verified in 3.4 sections, finding that $SO_4^{\cdot -}$ was main active species. In addition, previous study reported that GR nanomaterials showed comparable or better ability for the adsorption of organic pollutants than other carbonmaterials under NOM preloading [51]. It might suggest that the introduction of GR increased the adsorption of NOM by nZVI/GR, which decreased its inhibition on the generation of $SO_4^{\cdot -}$. However, as the concentration of NOM increased to 10 mg/L, atrazine degradation was inhibited. The degradation efficiency within 3 min decreased from 68.9% to 42.9% compared to the control, which was ascribed to the strong competitive scavenging of NOM.

3.4. Identification of dominant reactive species

To investigate the reactive species in the nZVI/GR-PS system, the spin-trapping ESR technique was used. As shown in Fig. 5a, the signals of DMPO-SO4 ($a_N = 13.7\, G$, $a_H = 10.0\, G$, $a_H = 1.41\, G$, and $a_H = 0.78\, G$) and DMPO-OH ($a_H = 15.0\, G$, $a_N = 14.9\, G$) were both observed from the typical hyperfine splitting constant in the nZVI-PS or nZVI/GR-PS system. The intensity of the DMPO-SO_4 signal in the nZVI-PS system was lower than that in the nZVI/GR-PS system, which was in good accordance with the result that the degradation efficiency of atrazine was better in nZVI/GR-PS system. This might be due to the fact that the electron transfer via C—OH and COOH groups on the surface of rGO accelerated the generation of $SO_4^{\cdot-}$ [41]. In addition, the intensity of the DMPO-SO_4 signal was stronger than that of DMPO-OH signal in the nZVI/GR-PS system. To deepen insight into the contributions of $SO_4^{\cdot-}$ and ·OH on atrazine degradation in the nZVI/GR-PS system, the quenching experiments were employed (Fig. 5b). It was reported that MeOH was used to scavenge both $SO_4^{\cdot-}$ and ·OH ($k_{SO4}{}^{\cdot-} = 0.9–1.3 \times 10^7\,M^{-1}\,s^{-1}$, $k_{\cdot OH} = 8.0–10 \times 10^8\,M^{-1}\,s^{-1}$) [52], while TBA mainly reacted with ·OH ($k_{SO4}{}^{\cdot-} = 4.0–9.1 \times 10^5\,M^{-1}\,s^{-1}$, $k_{\cdot OH} = 3.8–7.6 \times 10^8\,M^{-1}\,s^{-1}$) [24]. In the presence of 50 mM TBA and MeOH, the degradation efficiencies of atrazine after 61 min declined from 95.5% to 81.3% and 51.7% compared to the control, respectively. The inhibition was enhanced with increasing their dosages. Moreover, MeOH showed significant inhibitory effect on atrazine degradation than TBA. Besides, phenol was a more effective quenching agent for ·OH and $SO_4^{\cdot-}$ due to its high reactivity ($k_{SO4}{}^{\cdot-} = 6.6 \times 10^9\,M^{-1}\,s^{-1}$, $k_{\cdot OH} = 8.8 \times 10^9\,M^{-1}\,s^{-1}$) [53]. Compared to 50 mM MeOH or TBA, atrazine degradation was completely inhibited by 50 mM phenol. Even at 5.0 mM phenol, the degradation efficiency of atrazine was only 6.8%. It was attributed to the hydrophobic property of phenol, so it is easier to approach the surface of catalyst [54]. Hence, it could be concluded that both ·OH and $SO_4^{\cdot-}$ mainly occurred on the nZVI/GR surface, while $SO_4^{\cdot-}$ was the predominant radicals responsible for atrazine degradation.

3.5. *Degradation mechanisms and transformation pathways*

3.5.1. *Degradation mechanisms*

To elucidate the activation mechanism, nZVI/GR before and after reaction was analyzed by XRD and XPS techniques. After reaction, the peak corresponding to nZVI at 44.5° disappeared (Fig. 2a). Instead, the characteristic peaks "L" and "M" assigned to lepidocrocite and magnetite/maghemite were observed, respectively, indicating the oxidation of nZVI. This was further confirmed by XPS technique. As shown in Fig. 2b, the peaks of Fe$2p_{3/2}$ spectra located at 710.8 and 712.4 eV were assigned to Fe(II) and Fe(III), respectively. After reaction, the peak at 707.1 eV assigned to nZVI vanished, and the percentage of Fe(III) was increased from 54.4% to 60.3%, suggesting the oxidation of Fe(II) to Fe (III) via reacting with PS and O_2 on the surface of nZVI/GR. Zhu et al. [30] proposed that nZVI could react with H^+, O_2 and $S_2O_8^{2-}$ to generate Fe(II), which activated PS to yield $SO_4^{\cdot-}$ and conduced to the oxidation of DDT. Meanwhile, the concentration changes of dissolved Fe(II) and Fe(III) in the nZVI/GR-PS system were monitored. As shown in Fig. 6, the concentrations of Fe(II) and Fe(III) increased gradually and reached 7.05 mg/L and 9.88 mg/L after 61 min, respectively. These results indicated that nZVI would transform into the dissolved Fe(II), and further activated PS to degrade atrazine. In addition, the corrosion products of nZVI (lepidocrocite and magnetite/maghemite) might also stimulate PS decomposition. Both ·OH and $SO_4^{\cdot-}$ were identified as dominant reactive species in the core-shell Fe-Fe_2O_3/PS process [55]. In addition, the role of GR in the nZVI/GR-PS system was also investigated by XPS (Fig. 2c). C 1 s spectra of nZVI/GR could be deconvoluted into five components assigning to C—C (284.7 eV), C—OH (285.6 eV), C=O (288.5 eV), C—O—C (286.6 eV), and O—C=O (289.0 eV), respectively. The percentages of C—C, C—OH, C—O—C, C=O, and O—C=O groups in nZVI/GR were 44.5%, 22.5%, 12.2%, 9.5%, and 11.3%, respectively. After reaction, their contents were 53.4%, 9.4%, 19.1%, 9.8%, and 8.3%, respectively. As expected, the decrease of C—OH and COOH groups on the surface of GR indicating GR might directly activate PS and acted as an electron shuttle to mediate electron transfer reactions. During PS activation, C—OH and COOH groups would transform into organic radicals (CO˙ and COO˙) to produce $SO_4^{\cdot-}$. Similar result was found by Hussain et al. [56], who reported that nZVI/biochar composites increased the generation of $SO_4^{\cdot-}$ and the degradation of nonylphenol due to the presence of oxygen functional groups and large surface area of biochar. Yan et al. [41] also showed that the C—OH and COOH groups on rGO surface played an important role on the release of organic radicals to generate $SO_4^{\cdot-}$.

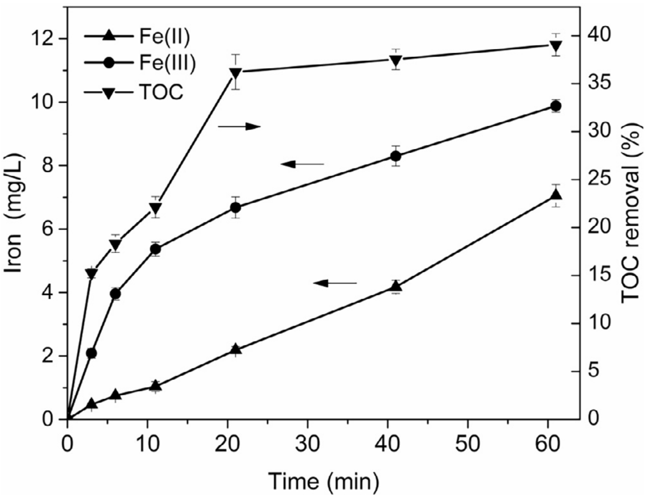

Fig. 6. The changes of Fe species and TOC in solution as a function of time. Conditions: [PS] = 0.50 mM, [nZVI/GR] = 0.10 g/L, [atrazine] = 10 mg/L, T = 25 °C, pH = 6.0.

Based on the above results, the activation mechanisms of PS by nZVI/GR w proposed (Scheme 1). The reactive sites of nZVI dispersed onto the surface of GR activated PS to generate $SO_4^{\cdot-}$ through the electron transfer from Fe(II) to PS, along with the corrosion product of nZVI produced. In addition, the oxygen-containing functional groups such as COOH and C—OH on the GR surface could act as electron shuttles and facilitate the transfer of electrons from GR to PS (Eqs. (10) and (11)), which would release organic radicals to yield $SO_4^{\cdot-}$. At last, $SO_4^{\cdot-}$ would further react with H_2O to generate ·OH. The synergistic effect between nZVI and GR for PS activation caused an efficient and rapid degradation of atrazine.

$$GR-OOH + S_2O_8^{2-} \rightarrow GR-OO^{\cdot} + SO_4^{\cdot-} + HSO_4^{-} \qquad (10)$$

$$GR-OH + S_2O_8^{2-} \rightarrow GR-O^{\cdot} + SO_4^{\cdot-} + HSO_4^{-} \qquad (11)$$

3.5.2. *Transformation pathways*

Besides, the mineralization of atrazine was determined by TOC analysis. Although the degradation efficiency of atrazine reached 92.1%, the removal of TOC was only 39.1% after 61 min (Fig. 6), which indicated that atrazine would transform into smaller molecules and underwent incomplete mineralization in the nZVI/GR-PS system. Thereby, the degradation intermediates of atrazine were detected by LC-MS/MS. As shown in Table S2, we identified 9 intermediate products based on their MS and MS^2 fragmentation. The main degradation pathways of atrazine in the nZVI/GR-PS system were illustrated in Scheme 2. First, $SO_4^{\cdot-}$ attacked the carbon adjacent to nitrogen by H-abstraction, leading to the formation of carbon-centered radical. Then, it was attacked by oxygen-producing peroxy radical and converted to atrazine-imine, and further the dealkylation products (CAIT, CEAT, OEAT, CAAT) were generated by path 1. In addition, the reaction of $SO_4^{\cdot-}$ with atrazine also occurred via electron transfer, thus resulting in the formation of the radical cation, along with dealkylation generated [47,57,58]. Most of atrazine (63%) was degraded based on $SO_4^{\cdot-}$ via dealkylation, and deethylation was more dominant than deisopropylation (10:1) [47]. Second, the carbon-centered radical was also attacked by ·OH to form alkylic hydroxylation products (CNTT, ODHT) by path 2. These two intermediates were also observed by Xu et al. [59], who conducted the degradation of atrazine using sono-photolysis

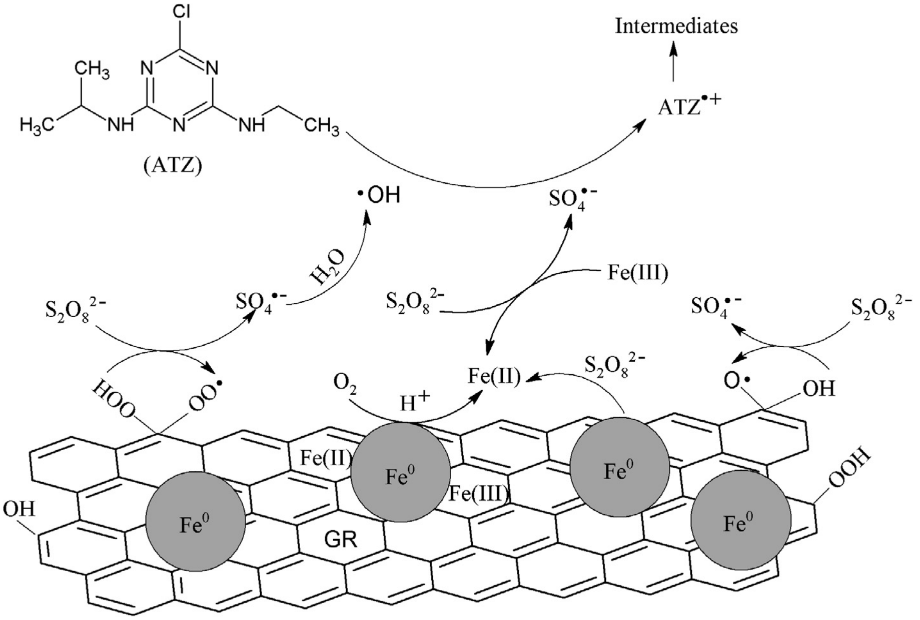

Scheme 1. Proposed mechanism of PS activation by nZVI/GR for atrazine degradation.

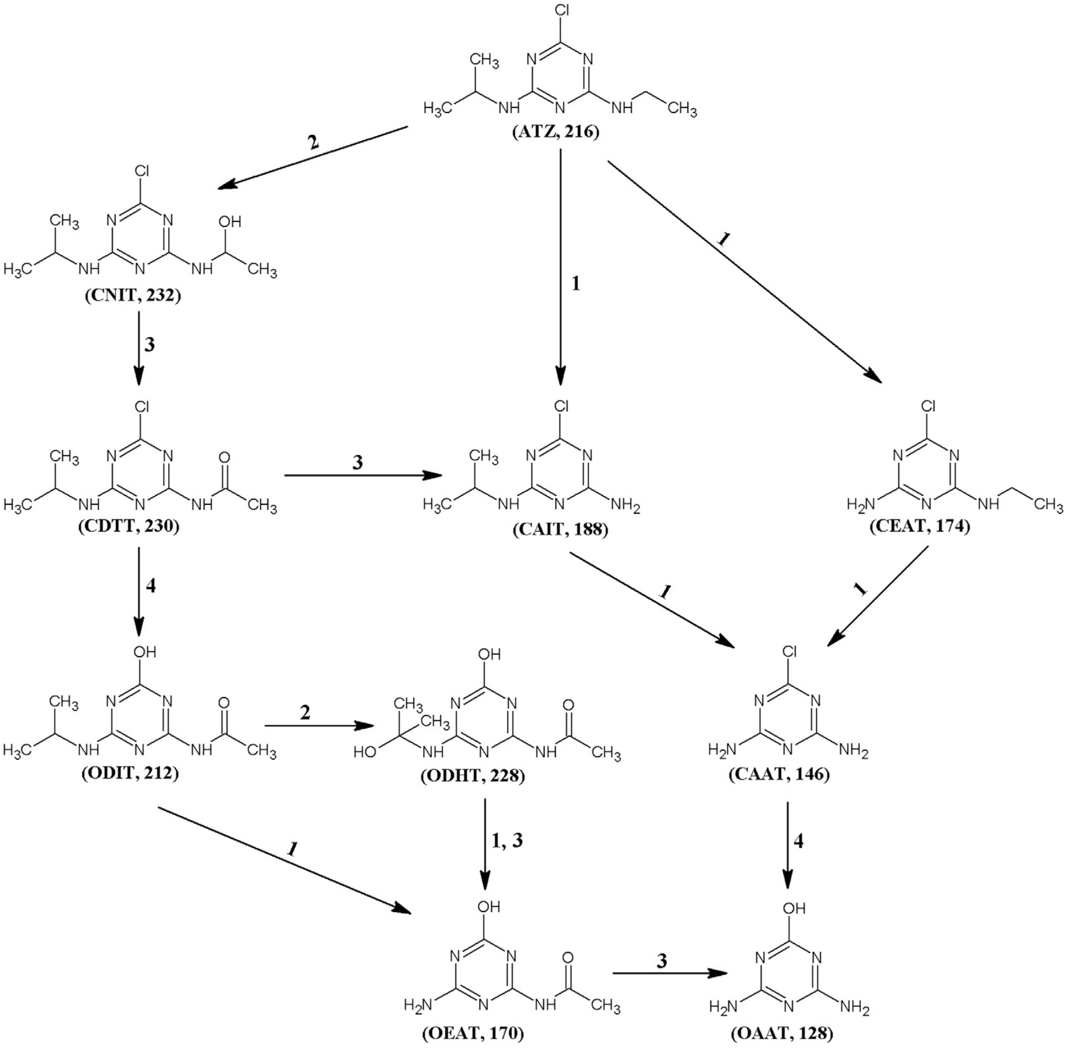

Scheme 2. The proposed degradation pathways of atrazine in the nZVI/GR-PS system. Dealkylation (1), alkylic hydroxylation (2), alkylic oxidation (3), and dechlorination- hydroxylation (4).

process. Especially, the transformation of ODIT to ODHT was verified by Kan et al. [60]. However, it was unstable and could be further oxidized by $SO_4^{\cdot -}/\cdot OH$ from H-abstraction, as described in Eq. (12) (path 3). Interestingly, ODHT underwent alkylic oxidition and dealkylation to form OEAT. Conversely, this confirmed the structure of $m/z = 170$ corresponded to OEAT, rather than 2-hydroxy-4-amino-6-isopropylamino-1,3,5-triazine obtained by Ji et al. [39]. The same pathway has been deduced by Xu et al. [59]. This reaction might be from a minor process because of the low concentration of ODHT. Furthermore, the degradation of atrazine proceeded through dechlorination- hydroxylation (path 4). It was reported that the C—Cl bond in atrazine was easy to be cleavaged due to the longest bond length (1.734 Å) and relatively low bond polarity (0.293) [61]. Ji et al. [39] proposed that the dechlorination-hydroxylation of atrazine was triggered by an intermediate HO-adduct radical. In summary, the degradation mechansims of atrazine included dechlorinatio-hydroxylation, dealkylation, alkylic hydroxylation, and alkylic oxidation.

$$RNHCHOHCH_3 + SO_4^{\cdot -}/\cdot OH \rightarrow RNHCOCH_3 \text{ (acetamide)} \qquad (12)$$

3.6. Application in actual water

Considering the further practical application, four different water simples spiked with atrazine were treated by nZVI/GR-PS system (Fig. 7). The degradation efficiency of atrazine in tap water was significantly decreased from 92.2% to 45.0% compared to that in milli-Q water. This was likely ascribed to the presence of inorganic anions, such as Cl^-, which reacted with $SO_4^{\cdot -}$ to generate other less active radicals (Eqs. (13–15)). Bennedsen et al. [62] reported that the removal of organic pollutants by nZVI/PS system could be strongly affected by Cl^- and HCO_3^-, acting as $SO_4^{\cdot -}$ scavengers and iron complexing agents. In lake water, the degradation of atrazine became worse, along with 40.1% of degradation produced, which was possibly induced by higher pH value, TOC, and high concentration of HCO_3^- and SO_4^{2-} (Table S3). Similar study was reported by Guan et al. [48], who found that the degradation of atrazine based on $SO_4^{\cdot -}$ and $\cdot OH$ in real water was mainly affected by TOC, pH, and alkalinity. Interesting, although the content of TOC in lake water was almost twice as much as river water, their degradation efficiency was almost the same. More research should be conducted to gain insight into the inhibition effects by inorganic anions in the nZVI/GR-PS system.

$$Cl^- + SO_4^{\cdot -} \rightarrow Cl^{\cdot -} + SO_4^{2-} \qquad (13)$$

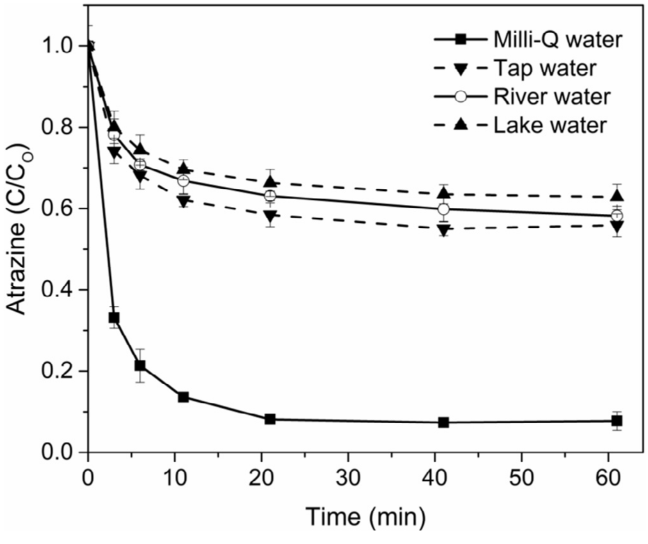

Fig. 7. The degradation of atrazine by nZVI/GR-PS system in real waters. Conditions: [PS] = 0.50 mM, [nZVI/GR] = 0.10 g/L, [atrazine] = 10 mg/L, T = 25 °C.

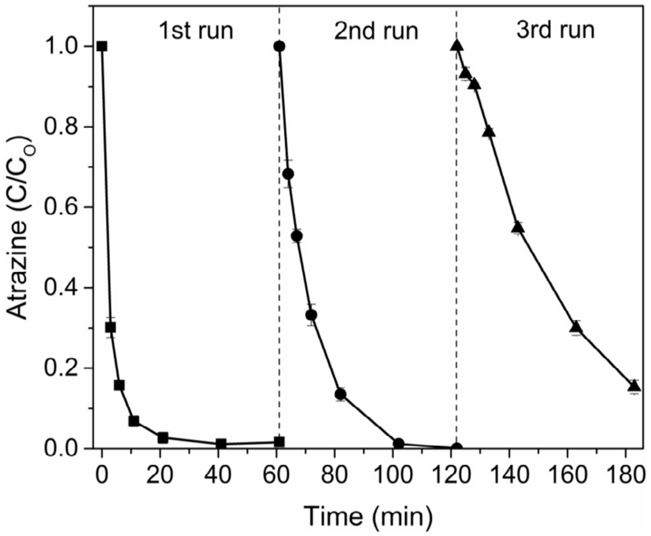

Fig. 8. The reusability of the nZVI/GR composite. Conditions: [nZVI/GR] = 0.10 g/L, [PS] = 0.50 mM, [atrazine] = 10 mg/L, T = 25 °C, pH = 6.0.

$$Cl^- + Cl^{\cdot -} \rightarrow Cl_2^{\cdot -} \qquad (14)$$

$$HCO_3^- + SO_4^{\cdot -} \rightarrow CO_3^{\cdot -} + SO_4^{2-} + H^+ \qquad (15)$$

3.7. Stability and reusability of nZVI/GR

The stability of nZVI/GR in the presence of PS was evaluated (Fig. 8). The degradation rate of the used nZVI/GR dropped considerably after each run, which might be attributed to the oxidation of nZVI. However, the degradation efficiency of atrazine still remained 84.7% in 3rd run. The above results showed that nZVI/GR-PS system could be a cost-effective, efficient and potential method for the degradation of atrazine with easy recycling and good stability.

4. Conclusions

The present work comprehensively explored the degradation of atrazine in the ZVI/GR-PS system. Several conclusions were drawn as below:

1) nZVI/GR with mass ratio of 5:1 achieved the highest degradation efficiency of 92.1% for atrazine removal within 21 min in the presence of PS.
2) The degradation of atrazine significantly increased with an increase of PS dose (< 1 mM), and was favored at acidic pH and high temperature, while was not affected by NOM with a concentration less than 4 mg/L. nZVI/GR would inhibit atrazine degradation when its dose increased to 200 mg/L.
3) Both $\cdot OH$ and $SO_4^{\cdot -}$ were mainly produced on the surface of nZVI/GR, while $SO_4^{\cdot -}$ was the dominant reactive species responsible for atrazine degradation.
4) On the basis of XPS and LC-MS/MS results, the mechanisms and pathways were proposed for atrazine degradation.
5) nZVI/GR-PS system showed excellent stability for atrazine degradation.

Acknowledgements

This work was supported by the National Natural Science Foundation of China (Grant No. 51478172, 51278464, 51521006), the International S&T Cooperation Program of China (Grant No. 2015DFG92750), the Natural Science Foundation of Zhejiang Province of China (Grant No. LY17E080002), the Natural Science Foundation of

Hunan Province of China (Grant No. 2017JJ2029), and the Department of Science and Technology of Changsha City of China (Grant No. kh1601187).

Appendix A. Supplementary data

Supplementary data associated with this article can be found, in the online version, at http://dx.doi.org/10.1016/j.cej.2018.01.136.

References

[1] R. Renner, Atrazine linked to endocrine disruption in frogs, Environ. Sci. Technol. 36 (2002) 55–56.
[2] D. Zhu, L. Jiang, R.L. Liu, P. Chen, L. Lang, J.W. Feng, S.J. Yuan, D.Y. Zhao, Wire-cylinder dielectric barrier discharge induced degradation of aqueous atrazine, Chemosphere 117 (2014) 506–514.
[3] A. Claver, P. Ormad, L. Rodríguez, J.L. Ovelleiro, Study of the presence of pesticides in surface waters in the Ebro river basin (Spain), Chemosphere 64 (2006) 1437–1443.
[4] R. Loos, G. Locoro, S. Comero, S. Contini, D. Schwesig, F. Werres, P. Balsaa, O. Gans, S. Weiss, L. Blaha, Pan-European survey on the occurrence of selected polar organic persistent pollutants in ground water, Water Res. 44 (2010) 4115–4126.
[5] C.P. Yang, H. Chen, G.M. Zeng, G.L. Yu, S.L. Luo, Biomass accumulation and control strategies in gas biofiltration, Biotechnol. Adv. 28 (2010) 531–540.
[6] W. Luo, C.P. Yang, H.J. He, G.M. Zeng, S. Yan, Y. Cheng, Novel two-stage vertical flow biofilter system for efficient treatment of decentralized domestic wastewater, Ecol. Eng. 64 (2014) 415–423.
[7] L. Katz, C.G. Dosoretz, R.T. Mandelbaum, M. Green, Atrazine degradation under denitrifying conditions in continuous culture of *Pseudomonas* ADP, Water Res. 35 (2001) 3272–3275.
[8] C. Desitti, U. Cheruti, M. Beliavski, S. Tarre, M. Green, Long-term atrazine degradation with microtube-encapsulated Pseudomonas sp. Strain ADP, Environ. Eng. Sci. 33 (2016) 167–175.
[9] L. Luo, H.J. He, C.P. Yang, S. Wen, G.M. Shan, M.J. Zeng, Z.L. Wu, W. Luo Zhou, Nutrient removal and lipid production by *Coelastrella* sp. in anaerobically and aerobically treated swine wastewater, Bioresour. Technol. 216 (2016) 135–141.
[10] S.H. Wu, H.J. He, X. Inthapanya, C.P. Yang, L. Lu, G.M. Zeng, Z.F. Han, Role of biochar on composting of organic wastes and remediation of contaminated soils-a review, Environ. Sci. Pollut. Res. 24 (2017) 16560–16577.
[11] Y.F. Ji, C.X. Dong, D.Y. Kong, J.H. Lu, Q.S. Zhou, Heat-activated persulfate oxidation of atrazine: implications for remediation of groundwater contaminated by herbicides, Chem. Eng. J. 263 (2015) 45–54.
[12] R.X. Li, C.P. Yang, H. Chen, G.M. Zeng, G.L. Yu, J.Y. Guo, Removal of triazophos pesticide from wastewater with Fenton reagent, J. Hazard. Mater. 167 (2009) 1028–1032.
[13] D.L. Huang, G.M. Zeng, C.L. Feng, S. Hu, X.Y. Jiang, T. Lin, F.F. Su, Y. Zhang, W. Zeng, H.L. Liu, Degradation of lead-contaminated lignocellulosic waste by *Phanerochaete chrysosporium* and the reduction of lead toxicity, Environ. Sci. Technol. 42 (2008) 4946–4951.
[14] Y. Zhang, Y. Cheng, C.P. Yang, W. Luo, G.M. Zeng, L. Lu, Performance of system consisting of vertical flow trickling filter and horizontal flow multi-soil-layering reactor for treatment of rural wastewater, Bioresour. Technol. 193 (2015) 424–432.
[15] T.T. Ye, Z.S. Wei, R. Spinney, C.J. Tang, S. Luo, R.Y. Xiao, D.D. Dionysiou, Chemical structure-based predictive model for the oxidation of trace organic contaminants by sulfate radical, Water Res. 116 (2017) 116–1106.
[16] Y. Cheng, H.J. He, C.P. Yang, G.M. Zeng, X. Li, H. Chen, G.L. Yu, Challenges and solutions for biofiltration of hydrophobic volatile organic compounds, Biotechnol. Adv. 34 (2016) 1091–1102.
[17] P. Neta, R.E. Huie, A.B. Ross, Rate constants for reactions of inorganic radicals in aqueous solution, J. Phys. Chem. Ref. Data 17 (1988) 1027–1284.
[18] C.P. Yang, H.Y. Liu, S.L. Luo, X. Chen, H.J. He, Performance of modified electro-Fenton process for phenol degradation using bipolar graphite electrodes and activated carbon, J. Environ. Eng. 137 (2012) 613–619.
[19] R.Y. Xiao, T.T. Ye, Z.S. Wei, S. Luo, Z.H. Yang, R. Spinney, Quantitative structure-activity relationship (QSAR) for the oxidation of trace organic contaminants by sulfate radical, Environ. Sci. Technol. 49 (2015) 13394–13402.
[20] S.L. Wang, N. Zhou, Removal of carbamazepine from aqueous solution using sono-activated persulfate process, Ultrason. Sonochem. 29 (2016) 156–162.
[21] C.W. Luo, J. Ma, J. Jiang, Y.Z. Liu, Y. Song, Y. Yang, Y.H. Guan, D.J. Wu, Simulation and comparative study on the oxidation kinetics of atrazine by UV/H_2O_2, UV/HSO_5^- and UV/$S_2O_82^-$, Water Res. 80 (2015) 99–108.
[22] Z.H. Yang, R.K. Su, S. Luo, R. Spinney, M.Q. Cai, R.Y. Xiao, Z.S. Wei, Comparison of the reactivity of ibuprofen with sulfate and hydroxyl radicals: an experimental and theoretical study, Sci. Total. Environ. 590–591 (2017) 751–760.
[23] O.S. Furman, A.L. Teel, R.J. Watts, Mechanism of base activation of persulfate, Environ. Sci. Technol. 44 (2010) 6423–6428.
[24] G.P. Anipsitakis, D.D. Dionysiou, Radical generation by the interaction of transition metals with common oxidants, Environ. Sci. Technol. 38 (2004) 3705–3712.
[25] P. Drzewicz, L. Perez-Estrada, A. Alpatova, J.W. Martin, M.G. El-Din, Impact of peroxydisulfate in the presence of zero valent iron on the oxidation of cyclohexanoic acid and naphthenic acids from oil sands process-affected water, Environ. Sci. Technol. 46 (2012) 8984–8991.
[26] G.D. Fang, D.D. Dionysiou, S.R. Al-Abed, D.M. Zhou, Superoxide radical driving the activation of persulfate by magnetite nanoparticles: implications for the degradation of PCBs, Appl. Catal. B-Environ. 129 (2013) 325–332.
[27] X.G. Duan, H.Q. Sun, J. Kang, Y.X. Wang, S. Indrawirawan, S.B. Wang, Insights into heterogeneous catalysis of persulfate activation on dimensional-structured nanocarbons, ACS Catal. 5 (2015) 4629–4636.
[28] H. Lee, H.J. Lee, J. Jeong, J. Lee, N.B. Park, C. Lee, Activation of persulfates by carbon nanotubes: oxidation of organic compounds by nonradical mechanism, Chem. Eng. J. 266 (2015) 28–33.
[29] H.R. Dong, Q. He, G.M. Zeng, L. Tang, L.H. Zhang, Y.K. Xie, Y.L. Zeng, F. Zhao, Degradation of trichloroethene by nanoscale zero-valent iron (nZVI) and nZVI activated persulfate in the absence and presence of EDTA, Chem. Eng. J. 316 (2017) 410–418.
[30] C.Y. Zhu, G.D. Fang, D.D. Dionysiou, C. Liu, J. Gao, W.X. Qin, D.M. Zhou, Efficient transformation of DDTs with persulfate activation by zero-valent iron nanoparticles: a mechanistic study, J. Hazard. Mater. 316 (2016) 232–241.
[31] L. Zhao, Y. Ji, D. Kong, J. Lu, Q. Zhou, X. Yin, Simultaneous removal of bisphenol A and phosphate in zero-valent iron activated persulfate oxidation process, Chem. Eng. J. 303 (2016) 458–466.
[32] S.Y. Oh, H.W. Kim, J.M. Park, H.S. Park, C. Yoon, Oxidation of polyvinyl alcohol by persulfate activated with heat, Fe^{2+}, and zero-valent iron, J. Hazard. Mater. 168 (2009) 346–351.
[33] H. Wang, X.Z. Zhong, Y. Wu, X.H. Chen, L.J. Leng, H. Wang, H. Li, G.M. Zeng, Facile synthesis of polypyrrole decorated reduced graphene oxide-Fe_3O_4 magnetic composites and its application for the Cr(VI) removal, Chem. Eng. J. 262 (2015) 597–606.
[34] Y. Zhu, S. Murali, W.W. Cai, X.S. Li, W.S.J.W. Suk, J.R. Potts, R.S. Ruoff, Graphene and graphene oxide: synthesis, properties, and applications, Adv. Mater. 22 (2010) 3906–3924.
[35] X. Li, L. Ai, J. Jing, Nanoscale zerovalent iron decorated on graphene nanosheets for Cr(VI) removal from aqueous solution: surface corrosion retard induced the enhanced performance, Chem. Eng. J. 288 (2015) 789–797.
[36] M. Xing, L.J. Xu, J.L. Wang, Mechanism of Co(II) adsorption by zero valent iron/graphene nanocomposite, J. Hazard. Mater. 301 (2016) 286–296.
[37] A. Ahmad, X.G. Gu, L. Li, S.G. Lv, Y.S. Xu, X.H. Guo, Efficient degradation of trichloroethylene in water using persulfate activated by reduced graphene oxide-iron nanocomposite, Environ. Sci. Pollut. Res. 22 (2015) 17876–17885.
[38] W.S. Hummers, R.E. Offeman, Preparation of graphitic oxide, J. Am. Chem. Soc. 80 (1958) 1339-1339.
[39] Y.F. Ji, C.X. Dong, D.Y. Kong, J.H. Lu, New insights into atrazine degradation by cobalt catalyzed peroxymonosulfate oxidation: kinetics, reaction products and transformation mechanisms, J. Hazard. Mater. 285 (2015) 491–500.
[40] Z.J. Li, L. Wang, L.Y. Yuan, C.L. Xiao, L. Mei, L.R. Zheng, J. Zhang, J.H. Yang, Y.L. Zhao, Z.T. Zhu, Z.F. Chai, W.Q. Shi, Efficient removal of uranium from aqueous solution by zero-valent iron nanoparticle and its graphene composite, J. Hazard. Mater. 290 (2015) 26–33.
[41] J.C. Yan, W.G. Gao, M.G. Dong, L. Han, L.B. Qian, C.P. Nathanail, M.F. Chen, Degradation of trichloroethylene by activated persulfate using a reduced graphene oxide supported magnetite nanoparticle, Chem. Eng. J. 295 (2016) 309–316.
[42] L. Bekris, Z. Frontistis, G. Trakakis, L. Sygellou, C. Galiotis, D. Mantzavinos, Graphene: a new activator of sodium persulfate for the advanced oxidation of parabens in water, Water Res. 126 (2017) 111–121.
[43] Z.H. Diao, X.R. Xu, D. Jiang, L.J. Kong, Y.X. Sun, Y.X. Hu, Q.W. Hao, H. Chen, Bentonite-supported nanoscale zero-valent iron/persulfate system for the simultaneous removal of Cr(VI) and phenol from aqueous solutions, Chem. Eng. J. 302 (2016) 213–222.
[44] S. Ahmed, M.G. Rasul, R. Brown, M.A. Hashib, Influence of parameters on the heterogeneous photocatalytic degradation of pesticides and phenolic contaminants in wastewater: a short review, J. Environ. Manage. 92 (2011) 311–330.
[45] X.Y. Wei, N.Y. Gao, C.J. Li, Y. Deng, S.Q. Zhou, L. Li, Zero-valent iron (ZVI) activation of persulfate (PS) for oxidation of bentazon in water, Chem. Eng. J. 285 (2016) 660–670.
[46] H.V. Lutze, S. Bircher, I. Rapp, N. Kerlin, R. Bakkour, M. Geisler, C.V. Sonntag, T.C. Schmidt, Degradation of chlorotriazine pesticides by sulfate radicals and the influence of organic matter, Environ. Sci. Technol. 49 (2015) 1673–1680.
[47] Y.H. Guan, J. Ma, Y.M. Ren, Y.L. Liu, J.Y. Xiao, L.Q. Lin, C. Zhang, Efficient degradation of atrazine by magnetic porous copper ferrite catalyzed peroxymonosulfate oxidation via the formation of hydroxyl and sulfate radicals, Water Res. 47 (2013) 5431–5438.
[48] I. Michael-Kordatou, C. Michael, X. Duan, X. He, D.D. Dionysiou, M.A. Mills, D. Fatta-Kassinos, Dissolved effluent organic matter: characteristics and potential implications in wastewater treatment and reuse applications, Water Res. 77 (2015) 213–248.
[49] S. Wen, H.Y. Liu, H.J. He, L. Luo, X. Li, G.M. Zeng, Z.L. Zhou, W. Lou, C.P. Yang, Treatment of anaerobically digested swine wastewater by *Rhodobacter blasticus* and *Rhodobacter capsulatus*, Bioresour. Technol. 222 (2016) 333–338.
[50] G.D. Fang, J. Gao, D.D. Dionysiou, C. Liu, D.M. Zhou, Activation of persulfate by quinones: free radical reactions and implication for the degradation of PCBs, Environ. Sci. Technol. 47 (2013) 4605–4611.
[51] L.H. Jiang, Y.G. Liu, S.B. Liu, G.M. Zeng, X.J. Hu, X. Hu, Z. Guo, X.F. Tan, L.L. Wang, Z.B. Wu, Adsorption of estrogen contaminants by graphene nanomaterials under NOM preloading: comparison with carbon nanotube, biochar and activated carbon, Environ. Sci. Technol. 51 (2017) 6352–6359.
[52] H. Eibenberger, S. Steenken, P. O'Neill, D. Schulte-Frohlinde, Pulse radiolysis and electron spin resonance studies concerning the reaction of $SO_4^{\bullet-}$ with alcohols and

ethers in aqueous solution, J. Phys. Chem. 82 (1978) 749–750.
[53] H.Y. Liang, Y.Q. Zhang, S.B. Huang, I. Hussain, Oxidative degradation of p -chloroaniline by copper oxidate activated persulfate, Chem. Eng. J. 218 (2013) 384–391.
[54] J. Zhang, X.T. Shao, C. Shi, S.Y. Yang, Decolorization of acid orange 7 with peroxymonosulfate oxidation catalyzed by granular activated carbon, Chem. Eng. J. 232 (2013) 259–265.
[55] L.L. Zhu, Z.H. Ai, W.K. Ho, L.Z. Zhang, Core-shell Fe–Fe_2O_3 nanostructures as effective persulfate activator for degradation of methyl orange, Sep. Purif. Technol. 108 (2013) 159–165.
[56] I. Hussain, M.Y. Li, Y.Q. Zhang, Y.C. Li, S.B. Huang, X.D. Du, G.Q. Liu, W. Hayat, N. Anwar, Insights into the mechanism of persulfate activation with nZVI/BC nanocomposite for the degradation of nonylphenol, Chem. Eng. J. 311 (2017) 163–172.
[57] S. Luo, Z.S. Wei, D.D. Dionysiou, R. Spinney, W.P. Hu, L.Y. Chai, Z.H. Yang, T.T. Ye, R.Y. Xiao, Mechanistic insight into reactivity of sulfate radical with aromatic contaminants through single-electron transfer pathway, Chem. Eng. J. 327 (2017) 1056–1065.
[58] S. Luo, Z.S. Wei, R. Spinney, F.A. Villamena, D.D. Dionysiou, D. Chen, C.J. Tang, L.Y. Chai, R.Y. Xiao, Quantitative structure-activity relationships for reactivities of sulfate and hydroxyl radicals with aromatic contaminants through single-electron transfer pathway, J. Hazard. Mater. (2017), http://dx.doi.org/10.1016/j.jhazmat.2017.09. 024.
[59] L.J. Xu, W. Chu, N. Graham, Atrazine degradation using chemical-free process of USUV: analysis of the micro-heterogeneous environments and the degradation mechanisms, J. Hazard. Mater. 275 (2014) 166–174.
[60] J.A. Khan, X. He, N.S. Shah, H.M. Khan, E. Hapeshi, D. Fatta-Kassinos, D.D. Dionysiou, Kinetic and mechanism investigation on the photochemical degradation of atrazine with activated H_2O_2, $S_2O_8{}^{2-}$ and $HSO_5{}^{-}$, Chem. Eng. J. 252 (2014) 393–403.
[61] C. Chen, S.G. Yang, Y.P. Guo, C. Sun, C.G. Gu, B. Xu, Photolytic destruction of endocrine disruptor atrazine in aqueous solution under UV irradiation: products and pathways, J. Hazard. Mater. 172 (2009) 675–684.
[62] L.R. Bennedsen, J. Muff, E.G. Søgaard, Influence of chloride and carbonates on the reactivity of activated persulfate, Chemosphere 86 (2012) 1092–1097.